m_{BPSK} = 3%. The modulation depth of the other 59 channels is 3.8%. A BER < 10^{-9} is achieved for modulation depths higher than 2.2%.

Using a spectrum analyser, we measured the composite second order (CSO) at various channels as a function of the modulation depth of the BPSK signal with the modulation depth for each of the analogue channels set at 3.8%. The distortion arises from the nonlinearity of the laser producing higher order harmonics and frequency mixing. Fig. 2 shows the CSO and composite triple beat (CTB) against the modulation depth of the BPSK signal. The data are shown for channel 14.

The distortion measurements are carried out using both short and long fibres to determine if there is a significant fibre induced distortion. Fig. 2 presents the distortion of the system with short POF (0.5m) and long POF (200m), respectively. The solid points are for 200m POF and the open circles are for 0.5m POF. The measured distortion curves using different length fibres for each channel are close to each other, suggesting that the fibre induced distortion is small.

The nonlinearity due to the BPSK signal can be calculated using the Gaussian approximation of Saleh [7]. The change in carrier to nonlinear distortion ratio (C/NLD) is given by

$$\Delta\left(\frac{C}{NLD}\right) = -20\log\left(1+\frac{m_{BPSK}^2}{4Nm^2}\right)$$

where N is the number of channels, each modulated with modulation depth m. For m_{BPSK} = 40%, N = 60, and m = 3.8%, the change in distortion using the above equation is 3.2dB, in qualitative agreement with the data measured.

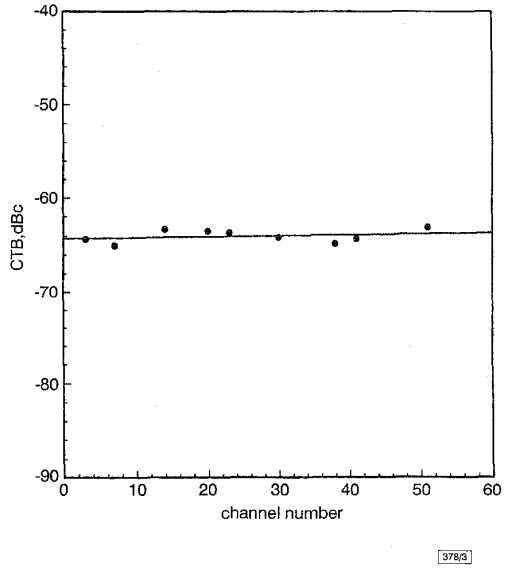

Fig. 3 *Measured CTB for various channels*

The CTB for various channels is shown in Fig. 3. The measured CTB is ~–64dBc for all channels. A similar result for the measured CSO with a value of ~–63dBc for all channels has been observed. The modulation depth of the analogue channel for this measurement was 3.8% and that of the BPSK channel was 3%. The fibre length is 200m.

In summary, the results of a transmission experiment using a hybrid AM/BPSK polymer optical fibre transmission system have been presented. A BPSK modulated 2Mbit/s pseudorandom digital channel is substituted for one of the AM channels in a 60 channel cable TV system. A bit error rate < 10^{-9} is obtained for a subcarrier modulated digital channel after transmission through 200m of fibre. The intermodulation distortion (IMD) effects using long and short fibre lengths have been studied. The results show that distortion caused by the laser nonlinearity did not degrade the system at low modulation depth. However, as the modulation depth of the BPSK signal is increased, the distortion is more pronounced. The differences between the measured IMDs for the long and the short fibre are negligible, suggesting that the fibre induced distortion in the transmission system is small.

28 August 1998
Electronics Letters Online No: 19981426

H. Fan, M.B. Tayahi, D.W. Young and N.K. Dutta (*Department of Physics and Photonics Research Center, University of Connecticut, Storrs, CT 06269, USA*)

R. Webster (*Boston Optical Fiber, Westborough, MA 01581, USA*)

References

1 CHIDDIX, J.A., LAOR, H., PANGRAC, D.M., WILLIAMSON, L.D., and WOLFE, R.W.: 'AM video on fiber in CATV systems: Need and implementation', *IEEE J. Sel. Areas Commun.*, 1990, **SAC-8**, (7), pp. 1229–1239

2 FREEMAN, P.N., and DUTTA, N.K.: 'Intermodulation distortion for a hybrid AM-VSB/digital system using a 1.55-μm laser and an optical amplifier', *IEEE Photonics Technol. Lett.*, 1996, **8**, (11), pp. 1558–1560

3 ISHIGURE, T., NIHEI, E., and KOIKE, Y.: 'Graded-index polymer optical fiber for high-speed data communication', *Appl. Opt.*, 1994, **33**, pp. 4261–4266

4 SHI, Q.: 'Asymptotic clipping noise distribution and its impact on M-ary QAM transmission over optical fiber', *IEEE Trans.*, 1995, **COM-43**, (6), pp. 2077–2084

5 JUNG, P., BAIER, P.W., and STEIL, A.: 'Advantages of CDMA and spread spectrum techniques over FDMA and TDMA in cellular mobile radio applications', *IEEE Trans.*, 1993, **VT-42**, (3), pp. 357–364

6 JOHANNSEN, K.G.: 'Code division multiple access versus frequency division multiple access channel capacity in mobile satellite communication', *IEEE Trans.*, 1990, **VT-39**, (1), pp. 17–26

7 SALEH, A.: 'Fundamental limit on number of channels in subcarrier multiplexed lightwave CATV system', *Electron. Lett.*, 1989, **25**, (12), pp. 770–777

Baud sampling bit synchroniser for channels with data dependent noise

A. Gameiro

A bit synchronisation algorithm for channels with data dependent noise which operates with one sample per symbol is presented. The algorithm uses the same information as the Mueller and Müller (M&M) algorithm, and is optimised for operation with data dependent noise. The performance is derived and it is shown that significant improvements over the M&M algorithm can be obtained in practical optical channels.

Introduction: In this Letter we deal with bit synchronisation in channels with data dependent noise. Examples of such channels arise in optical communications using APD (avalanche photodiode) receivers, or direct detection of optically amplified signals [1]. In such systems the noise power is higher when a logical one is received. Another situation where data dependent noise arises is in the detection of signals in the presence of clutter [2, 3].

Although the problem of detection in asymmetric noise has received considerable attention in optical communications [4] and other channels [3], much less attention has been devoted to the problem of synchronisation [2]. In this Letter, we consider the operation of an error tracking synchroniser operating with one sample per symbol in a channel with data dependent additive noise. We start with the popular Mueller and Müller algorithm (M&M) [5], which is widely used in digital modems, and modify it to take advantage of the noise data dependence. The variance of the tracking error is derived and the two algorithms compared. A numerical example with a direct detection optical receiver shows that significant improvements may be obtained in practical situations.

System model: Digital receivers operate on samples of the received continuous-time signal. The generic structure of an error tracking baud sampling bit synchroniser [6] with synchronised sampling is shown in Fig. 1. The sampling instants, $t_k = kT + \hat{\tau}_k$, given by a numerically controlled oscillator (NCO) are adjusted by the filtered output of the timing error detector.

The sample y_k at time $t_k = kT + \hat{\tau}$, corresponding to an estimate $\hat{\tau}$ of delay, is given by

$$y_k = \sum_m a_{k-m} g(mT + \tau - \hat{\tau}) + n_k(a_k) \quad (1)$$

where $\{a_k\}$ is a sequence of independent random variables taking the values –1 and +1 with equal probability; $1/T$ is the bit rate; $g(t)$ is the baseband elementary pulse and τ is the true delay to be tracked.

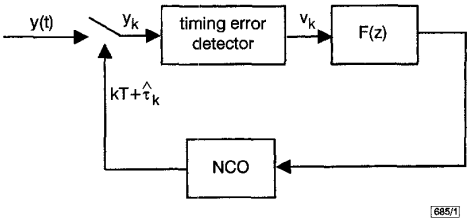

Fig. 1 *Generic structure of baud sampling error tracking symbol synchroniser*

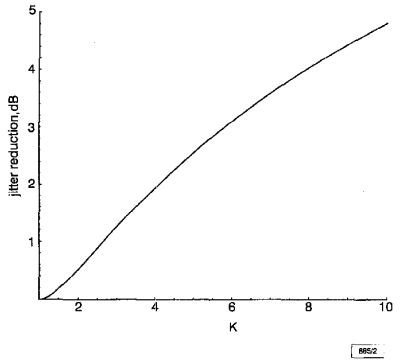

Fig. 2 *Jitter reduction achieved with new algorithm against ratio K*

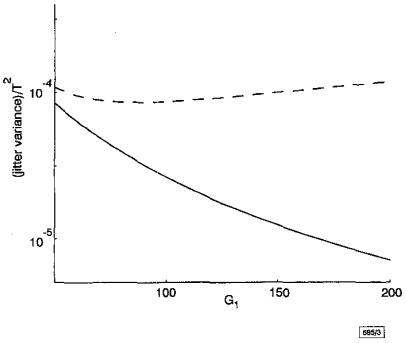

Fig. 3 *Jitter variance for M&M and new algorithms against APD gain G_1*

——— modified algorithm
– – – – M&M

For the noise model, we consider that the noise samples $n_k(a_k)$ form a sequence of independent zero mean Gaussian noise variables, with variance equal to σ_1^2 when $a_k = 1$ and σ_{-1}^2 when $a_k = -1$. We define the following parameters to be used in the following Sections: the average noise power

$$\sigma_{av}^2 = (\sigma_1^2 + \sigma_{-1}^2)/2 \quad (2)$$

and the variance ratio

$$K = \sigma_1^2/\sigma_{-1}^2 \quad (3)$$

M&M algorithm: The timing error detector for the M&M algorithm is defined as

$$v_k = y_k a_{k-1} - y_{k-1} a_k \quad (4)$$

and the timing error characteristic is [5]

$$s(\hat{\tau} - \tau) = E[v_k(\hat{\tau})|\tau] = g(\hat{\tau} - \tau + T) - g(\hat{\tau} - \tau - T) \quad (5)$$

For ISI free pulses, the equilibrium point is $\hat{\tau} = \tau$ and the algorithm is pattern-jitter free. The variance of the linearised timing error can be computed using the general result [6]

$$E[(\hat{\tau} - \tau)^2] = 2B_L T \frac{S_d(1)}{(s'(0))^2} \quad (6)$$

where $S_d(z)$ is the Z transform of the disturbance autocorrelation at the equilibrium point, and B_L is the one sided loop noise bandwidth. For our channel model we obtain

$$E\left[\frac{(\hat{\tau} - \tau)^2}{T^2}\right] = B_L T \frac{\sigma_{av}^2}{(Tg'(T))^2} \quad (7)$$

Modified algorithm for data dependent noise: Eqn. 7 shows that the M&M algorithm discards the data dependent nature of the additive noise. The timing error variance is identical to the variance that would be obtained with independent additive noise of variance σ_{av}^2. To take advantage of the noise-data dependence, we consider the following modified algorithm that uses the same samples and the same regenerated data symbols of the M&M algorithm:

$$v_k = (y_k - a_k)F(a_{k-1}, a_k) - (y_{k-1} - a_{k-1})F(a_k, a_{k-1}) \quad (8)$$

where $F(.)$ is some discrete function we want to optimise. The corresponding timing error characteristic is

$$s(\hat{\tau} - \tau) = E[a_{k-1}F(a_{k-1}, a_k)]\,(g(\hat{\tau} - \tau + T) - g(\hat{\tau} - \tau - T)) \quad (9)$$

For ISI free elementary pulses the equilibrium point is at $\tau = \hat{\tau}$, and the disturbance at this point is given by

$$d_{nk} = n_k(a_k)F(a_{k-1}, a_k) - n_{k-1}(a_{k-1})F(a_k, a_{k-1}) \quad (10)$$

From eqn. 6, the linearised phase error variance is proportional to $S_d(1)/(s'(0))^2$, and performing the computations gives

$$\frac{S_d(1)}{(s'(0))^2} = \frac{4(\sigma_1^2(F(1,1) - F(-1,1))^2 + \sigma_{-1}^2(F(1,-1) - F(-1,-1))^2)}{(F(1,1) + F(-1,1) - F(1,-1) - F(-1,-1))^2} \quad (11)$$

Minimisation of eqn. 11 is readily accomplished, and we find that there is no unique solution. Any choice for the four values of $F(.)$ that verify the condition

$$F(1,-1) - F(-1,-1) = K(F(1,1) - F(-1,1)) \quad (12)$$

is suitable and leads to the minimum variance

$$E\left[\frac{(\hat{\tau} - \tau)^2}{T^2}\right] = B_L T \frac{\sigma_{av}^2}{(Tg'(T))^2} \frac{4K}{(1+K)^2} \quad (13)$$

Among the set of solutions specified by eqn. 12, the choice

$$\begin{cases} F(1,1) = -F(-1,1) \\ F(1,-1) = -F(-1,-1) = KF(1,1) \end{cases} \quad (14)$$

leads to uncorrelated disturbance samples, and represents the intuitively expected solution, that the M&M algorithm should be modified by giving more weight to the samples corresponding to a reduced noise variance.

In Fig. 2 we plot the reduction in the jitter variance given by the new algorithm relative to the M&M against ratio K. The plot shows that significant improvements may be obtained if there is a large asymmetry in the noise powers. In Fig. 3, we evaluate the jitter variance for the M&M and for the new algorithm in an optical communication system with an APD receiver, against the APD gain G_1. The transmission parameters used for the computations are given in Table 1. The received optical pulse was assumed to be rectangular with duration T and the electrical equaliser considered to be matched to this pulse. The APD excess noise factor was computed using the relation

$$F = \gamma G_1 + \left(2 - \frac{1}{G_1}\right)(1 - \gamma)$$

with $\gamma = 0.028$.

The plot shows that significant improvements are obtained by resorting to the new algorithm. Furthermore, the new algorithm allows higher APD gains than the M&M, which exhibits an optimum APD gain beyond which the jitter variance increases.

Table 1: Transmission parameters

Bit rate	R = 100Mbit/s
Input average optical power	P_{av} = –50dBm
Quantum efficiency	$\eta = 1$
Extinction ratio	$\varepsilon = 0$
Wavelength	λ = 1300nm
Input noise current	$(E[i_n^2])^{1/2}$ = 4pA/√Hz
Loop bandwidth	$B_L T = 0.01$

Conclusions: In this Letter a new baud sampling timing error detector suitable for channels with data dependent noise was presented. The new algorithm uses the same information as the well-known M&M algorithm, but gives more emphasis to the signal samples corrupted by low noise. The linearised performance was derived, and the results show that significant improvements may be obtained if there is a high level of asymmetry between the noise levels. A numerical example with an APD based optical receiver was presented showing that considerable gains may be obtained in practical optical communication systems.

20 July 1998
Electronics Letters Online No: 19981437

A. Gameiro (*Department of Electronics and Telecommunications, University of Aveiro, 3810 Aveiro, Portugal*)

E-mail: amg@ua.pt

References

1 GAGLIARDI, R.M., and KARP, S.: 'Optical communications' (Wiley, 2nd. Edn. 1995)
2 TSANG, C.S., and LINDSEY, W.C.: 'Bit synchronisation in the presence of asymmetric channel noise', *IEEE Trans. Commun.*, 1986, pp. 528–537
3 MARAS, A.M., and KOKKINOS, E.A.: 'Locally optimum Bayes detection (LOBD) in signal-dependent noise', *IEEE Trans. Commun.*, 1997, pp. 523–526
4 TANG, J., and BEN LETAIEF , K.: 'The use of WMC distribution for performance evaluation of APD optical communication systems', *IEEE Trans. Commun.*, 1998, pp. 279–285
5 MUELLER, K.H., and MÜLLER, M.: 'Timing recovery in digital synchronous data receivers', *IEEE Trans. Commun.*, 1976, pp. 516–530
6 MEYR, H., MOENECLAEY, M., and FECHTEL, S.A.: 'Digital communication receivers' (Wiley, 1998)

Choice of standard medium temperature for tropical and equatorial climates: Comparison between radiometric and satellite beacon attenuation data on two 12GHz links in Brazil

E. Couto de Miranda, M.S. Pontes, L.A.R. da Silva Mello and M.P. de Almeida

Results are presented for two years of satellite beacon and radiometric attenuation measurements on two 12GHz Earth-space links located in Rio de Janeiro, south-eastern Brazil and Belém, northern Brazil. Results suggest that the choice of 285K for the standard medium temperature, to be used in the calculation of attenuation from radiometric measurements of sky temperature, may underestimate the conditions for tropical and equatorial environments.

Introduction: Rainfall induced attenuation is the main cause of impairment to satellite communications above 10GHz, even more so in tropical and equatorial climates in which heavy rainfall events are common. Since the majority of the studies on Earth-space propagation have been conducted in Europe and the USA, the existing prediction models may not be sufficiently accurate to characterise the effects of attenuation in tropical and equatorial climates. This Letter aims not only to increase the available data on Earth-space propagation in tropical and equatorial climates, but also to suggest that the use of 285K as the standard medium temperature in the calculation of radiometric attenuation from sky noise temperature measurements may underestimate the conditions in tropical and equatorial environments.

Experimental setup: The receiver site in Rio de Janeiro (tropical with 2 – 3 dry months, ITU-R climate N) is located at co-ordinates 22°54′S, 43°15′W. The elevation angle is ~63° and the height above sea level is 30m. The receiver site in Belém (equatorial with no dry months, ITU-R climate N) is located at 01°27′S, 48°29′W. The elevation angle is ~ 89° and the height above sea level is 24m. The receiver antennas have diameters of 3m. The antennas are pointed towards INTELSAT 705, located at 50°W. The beacon frequency is 11.452GHz and it is clockwise circularly polarised. The beacon EIRP is 7dBw. The beacon signal has a narrow bandwidth due to the lack of modulation. Since all the energy is contained close to the centre frequency, the receiver was built with a narrow bandwidth, thus reducing the noise. The dynamic range of the receiver can therefore be large enough to allow the observation of severe attenuation events. The dual-slope radiometers operate at 12GHz and have antennas 1.2m in diameter. A tipping bucket raingauge with 0.1mm capacity and 1min integration time is placed near the antenna. The data are sampled at 1Hz and stored in a computer for downloading. High frequency noise is reduced by the analysis software, which smoothes the data by averaging over 2s, thus reducing the sampling rate from 1 to 2Hz. This sampling and logging computer is called the data acquisition unit (DAU). The DAU is designed for remote operation, allowing the deployment of several satellite beacon receiver units throughout the country for a more widespread coverage of different radioclimatic areas.

Motivations for work and brief theoretical background: The greatest advantage in using satellite beacon measurements over radiometers for measuring attenuation is that the range of possible attenuations is greatly increased, reaching values of 24dB and higher. Radiometers can only measure attenuation values up to 10dB before the readings diverge. In fact, radiometers measure sky noise temperature and it is from these measurements that the attenuation is obtained through a well known relationship [1]:

$$A\ [\mathrm{dB}] = 10 \log \left[\frac{(T_m - T_{cs})}{(T_m - T_{sky})} \right] \qquad (1)$$

where T_m is the standard medium temperature, T_{cs} is the clear sky reference temperature (in our case equal to 30K) and T_{sky} is the radiometric measured sky noise temperature, all measured in Kelvin. Eqn. 1 can be used to adjust the 'zero' of the beacon measurements [1] because the noise temperature is unaffected by atmospheric effects that cause fluctuations in the satellite beacon received power.

Establishing a zero level reference is not, however, the only possible result obtainable from the relationship between beacon and radiometric attenuation data. Inspecting eqn. 1, it is noticeable that the radiometric derived attenuation is a direct function of the standard medium temperature T_m. This parameter dictates the point from which the attenuation begins to diverge, or, in other words, the point above which the denominator becomes close to zero. A study by Allnut *et al.* [2] suggests the use of 285K for T_m, which places the divergence point close to 10dB. By comparing the cumulative probability distribution functions of beacon and radiometric attenuation at equiprobable levels it is possible to estimate the value of T_m which makes the percentile-percentile plot of the distributions closer to a straight line of unit slope. This was the procedure applied in this particular study and the results are presented in the following Section.

Results: As mentioned in the preceding Section, the procedure used in this study for obtaining the standard medium temperature is based on the comparison between equiprobable values of the